J. Appl. Comput. Mech., 12(4) (2026) 1535-1545
DOI: 10.22055/jacm.2026.48947.5616

ISSN: 2383-4536
jacm.scu.ac.ir

Shahid Chamran University of Ahvaz

Journal of Applied and Computational Mechanics

Research Paper

Nonlinear Dynamic Analysis of Composite Wind Turbine Blades using Lamination and Equivalent Beam Theory

Andres Lopez-Lopez[1], Rocio M. Sánchez-Albores[2], Perla Y. Sevilla-Camacho[3,4], Héctor H. Torres-Ventura[2], Juvenal Rodríguez-Resendíz[5], José B. Robles-Ocampo[3,6]

[1] Centro de Investigación, Innovación y Desarrollo Tecnológico, Universidad del Valle de México,Av. Marina Nacional 500, Anáhuac I Secc, Miguel Hidalgo, Ciudad de México, 11320, México, Email: andres.lopez@uvmnet.edu

[2] Escuela de Ciencias Químicas, Universidad Autónoma de Chiapas (UNACH), Ocozocoautla de Espinosa, Chiapas, CP 29140, México, Email: magdalena.sanchez@unach.mx (R.M.S.A.); hector.torres@unach.mx (H.H.T.V.)

[3] Cuerpo Académico de Energía y Sustentabilidad, Universidad Politécnica de Chiapas, Suchiapa 29150, México, Email: jrobles@upchiapas.edu.mx

[4] Programa Académico de Ingeniería Mecatrónica, Universidad Politécnica de Chiapas, Suchiapa 29150, México, Email: psevilla@upchiapas.edu.mx

[5] Facultad de Ingeniería, Universidad Autónoma de Querétaro, Cerro de las Campanas, Las Campanas, Querétaro C.P. 76010, México, Email: juvenal@uaq.edu.mx

[6] Programa Académico de Ingeniería en Manufactura Avanzada, Universidad Politécnica de Chiapas, Suchiapa 29150, México, Email: jrobles@upchiapas.edu.mx

Received November 27 2025; Revised February 13 2026; Accepted for publication February 17 2026.
✉ Corresponding author: J.B. Robles-Ocampo (jrobles@upchiapas.edu.mx)
© 2026 Published by Shahid Chamran University of Ahvaz

Abstract. This study develops and validates a nonlinear dynamic model for a 1.5 kW composite wind turbine blade prone to large deflections. The methodology combines an equivalent beam model that accounts for geometric nonlinearities and variable sectional properties with a numerical solution via the Runge-Kutta method. Experimental free- and forced-vibration tests on a cantilevered blade confirmed nonlinear stiffening, evidenced by spectral widening, a superharmonic resonance at 30.7 Hz, and asymmetric orbits in phase portraits. The model accurately predicts the global dynamic response, with errors below 8.6% in nonlinear regimes, providing a reliable tool for identifying critical frequencies and supporting the safe design of wind turbine blades.

Keywords: Composite wind turbine blade; geometric nonlinearity; nonlinear dynamics; equivalent beam theory, classical lamination theory.

1. Introduction

Composite Wind Turbine Blades (CWTB) are the primary component in capturing and transforming the kinetic energy of the wind into electrical energy. This transformation is achieved by rotating the rotor, which drives an electric generator. However, the CWTB design trend towards greater slenderness to maximize efficiency makes them highly flexible. The flexibility of CWTB, combined with its continuous operation under complex wind fields, results in strong coupling among aerodynamic, inertial, and elastic forces [1, 2]. Consequently, CWTBs exhibit nonlinear dynamic behavior characterized by large deformations and unstable vibrations.

This structural vulnerability is exacerbated by exposure to adverse environmental conditions, such as wind variability, waves (in offshore farms), and seismic events. Under these conditions, CWTBs experience significant vibrations, which, if excessive, can induce critical vibration modes. These oscillations not only reduce energy conversion efficiency but also cause structural damage. In the worst-case scenario, they can compromise the integrity of the entire Wind Turbine (WT), potentially leading to its collapse under extreme events [3, 4]. Therefore, the efficiency, safety, and longevity of a WT are directly determined by the dynamic characteristics of its CWTBs [5].

In a global context where WTs play a crucial role in producing clean, renewable energy, ensuring their reliability and operational efficiency is paramount. Predicting and controlling vibrations in CWTBs is therefore critical for preventing failures, ensuring structural integrity, and optimizing operational and maintenance costs. For these reasons, the development of efficient mathematical models, precise experimental methodologies, and advanced numerical simulations has become a priority research area for the analysis of the vibrational dynamics of CWTBs.

The study of the vibrational behavior of CWTBs has advanced through the development of analytical, numerical, and experimental models, delineating two main lines of research: mathematical modeling and numerical simulation, and non-destructive testing. Xu et al. [6] revealed that linear Euler-Bernoulli and Timoshenko beam models exhibit significant limitations in capturing geometric nonlinearities, especially when deflections exceed 10% of the blade length. This necessity has driven the

Published online: February 22 2026

incorporation of geometric nonlinearity to account for large deformations in slender structures. Thus, the work conducted by Gonzalez-Cruz et al. [7] laid the groundwork by validating simplified models with nonlinear terms, demonstrating phenomena such as frequency shifts and bifurcation jumps, and suggesting their adaptability to real-world CWTBs. On the other hand, Karimi and Moradi [8] demonstrated energy transfer between coupled flapwise and edgewise modes through the analysis of their frequency relationships. However, their model assumes homogeneous material, limiting its applicability to composite or non-homogeneous materials. Finally, Lang et al. [9] characterized nonlinear effects in the flapwise vibration of blades due to large deformations, identifying multipeak responses under a simplified harmonic load, F·cos(ωt), albeit without considering the actual composite structure of the CWTBs.

Subsequent research has developed more sophisticated models to overcome these limitations. On the one hand, there are nonlinear one-dimensional models, such as the one proposed in [10], which incorporated aerodynamic loads and damping and were experimentally validated in a wind tunnel; however, this research's one-dimensional nature prevents it from capturing the complexity of the three-dimensional geometry.

On the other hand, three-dimensional and multibody models aim to overcome this restriction. In [11], a three-dimensional analytical model for variable sections was developed and validated using the Finite Element Method (FEM), although it was limited to straight geometries. As complexity increases, the multibody model from Xue et al. [12], captures geometric nonlinearity and aeroelastic response with high precision, albeit at a high computational cost.

Concurrently, Navadeh et al. [13] employed the commercial finite element method (FEM) software (ABAQUS) to quantify the impact of geometric nonlinearity, observing a 15% increase in deflection. This study modeled a 44.175 m blade with variable cross-sections using the S4R shell element and identified nonlinear effects under pulsating loads. However, this work is considered a unidirectional material shell without incorporating the actual multilayer configuration. An intermediate approach was proposed by Jokar et al. [14], whose nonlinear model incorporated effects of rotational inertia and centrifugal forces. However, the linearization of free vibrations and the lack of experimental validation limit its practical applicability.

Concurrently, experimental validation and the development of non-destructive testing are crucial to ensure the relevance of these models. In this area, Lopez-Lopez et al. [15] proposed an innovative, non-destructive method for determining the dynamic modulus of elasticity with high precision by modeling the blade as an equivalent beam. Similarly, Ou et al. [16] subjected a 3.5 kW cantilever blade to shaker excitation, monitoring natural frequencies and damping ratios to assess damage. This study determined that damage sensitivity is specific to each vibrational mode and that there is no single universal modal indicator. A subsequent advance in research conducted by Aranizadeh et al. [17], used Power Spectral Density (PSD) analysis to identify cracks in 5 kW blades from their flapwise modes. However, this methodology did not account for the influence of nonlinear behavior on alterations in structural response.

This limitation is representative of a broader challenge. Although methods such as PSD have been employed to detect faults in small-scale Blades [18], their application has been limited by their inability to capture nonlinear phenomena and to integrate the complex behavior of laminated materials.

In a practical application, Jiménez et al. [19] proposed a simplified resonance excitation method to estimate the fatigue life of low-power wind turbines, achieving errors of less than 5%. However, its applicability to complex composite materials remains to be investigated. Concurrently, Sevilla-Camacho et al. [20] successfully integrated vibration analysis with Support Vector Machine (SVM) algorithms for the monitoring and fault detection of small CWTBs, achieving 98% accuracy. Finally, Ou et al. [21] established an experimental benchmark for damage detection, demonstrating the stability of modal properties against temperature variations.

The literature review reveals a fundamental trade-off in modeling CWTBs: the pursuit of high physical fidelity, such as detailed geometries, nonlinearities from large deformations, and anisotropic materials, versus the constraints of computational cost and experimental feasibility. While notable advances have been made in modeling geometric nonlinearities and developing validation techniques, a critical gap persists. There is a clear need to develop models that simultaneously capture large deformations and the anisotropy of the composite material, and that are supported by experimental methodologies ensuring a reliable correlation between simulations and real operational conditions.

The objective of this work is to develop and validate a computationally efficient numerical model to determine the nonlinear dynamic behavior of a CWTB. To this end, a one-dimensional model is proposed based on Lagrange's equations and a Rayleigh-Ritz displacement approximation, accounting for large flapwise deflections through geometric nonlinearity. The model incorporates composite material properties through a sectional analysis using Classical Lamination Theory (CLT), integrating the blade sections' elastic and inertial properties into a unified equivalent beam model. The model will be evaluated in free vibration for both small and large deflections, as well as in forced vibration with harmonic excitation of the form F·sin(ωt), to characterize its behavior under resonance conditions and in the presence of coupled modes. Finally, the model is validated on a cantilever beam test bench to characterize nonlinear effects and verify its accuracy against experimental results.

2. Materials and Methods

The methodology for the dynamic analysis of CWTBs (Fig. 1) consists of an iterative process integrating modeling, simulation, and experimental validation. The process begins with defining the blade's geometric and material properties, from which sectional properties are calculated to obtain an equivalent beam model that simplifies dynamic structural analysis. Subsequently, initial and boundary conditions are established to develop the nonlinear model, which accounts for the geometric nonlinearities of the CWTB deflection. With the model defined, numerical simulation is performed in two stages: free vibration and forced vibration. In parallel with numerical modeling, free- and forced-vibration tests are conducted on CWTB for validation. The results are compared with simulations using amplitude comparisons, following these criteria: if the error in free vibration exceeds 1%, the process restarts from the nonlinear modeling stage; whereas in forced vibration, the process is successfully completed only when the error is below 10%. If these criteria are not met, the model is iteratively recalibrated until the required precision is achieved.

2.1. Nonlinear modeling

Figure 2 shows a schematic of the CWTB model. To capture its dynamic behavior, the blade is modeled as a flexible cantilever beam with uniformly distributed mass and stiffness. The figure also depicts the $x-y$ reference frame, which lies in the plane perpendicular to the blade's rotation. L represents the undeformed length, w is the flapwise deflection, and θ denotes the deflection slope.

CWTBs experience maximum deflection at the tip end under high wind loads. The deformation of the CWTB's continuous system is represented by a series of normalized vibration modes, combined linearly, which allows for reducing the system's degrees of freedom from infinite to a finite number N, corresponding to the modes selected for analysis. Therefore, the deformation $W(x)$ of the flexible cantilever beam at any point along its length can be described as a linear superposition of normalized modes N_i.

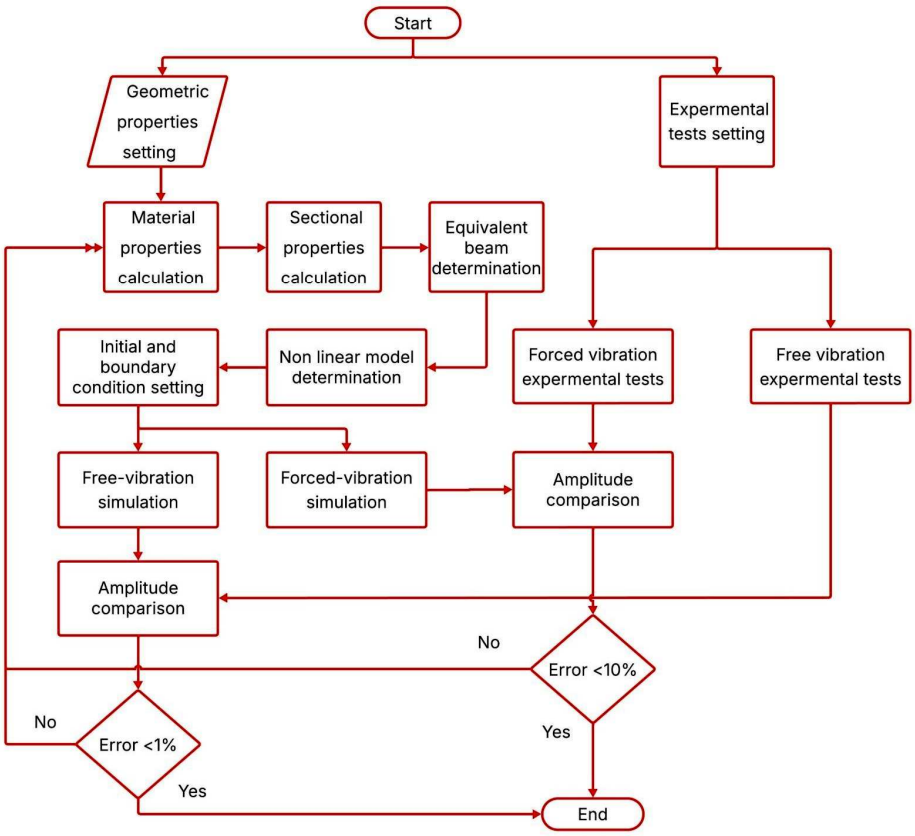

Fig. 1. Methodology for dynamic analysis of CWTB.

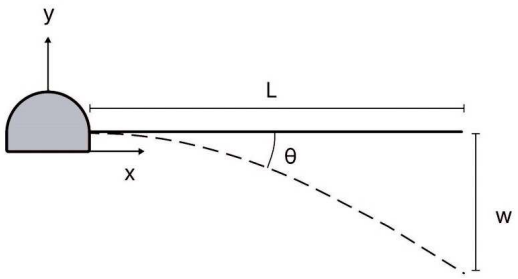

Fig. 2. Schematic of the CWTB cantilever model.

These modes are related to the generalized coordinates q_i by Eq. (1) [22]:

$$W = \sum_{i=1}^{n} N_i q_i \tag{1}$$

Suppose the CWTB is modeled as a one-dimensional, two-node element. Thus, the system is described by four generalized coordinates $\boldsymbol{q}$, the deflection w_i and bending slope θ_i at each node i (for $i = 1, 2$). This leads to four normalized modes, given by Eq. (2):

$$\boldsymbol{q} = [w_1, \theta_1, w_2, \theta_2] \tag{2}$$

When modeling the CWTB as a cantilever beam fixed at $x = 0$ and free at $x = L$, the boundary conditions simplify the displacements, which must satisfy (see Eq. (3)):

$$\begin{aligned} w(0) = w_1 = 0 \quad & \frac{\partial w(0)}{\partial y} = \theta_1 = 0 \\ w(L) = w_2 = w \quad & \frac{\partial w(L)}{\partial y} = \theta_2 = \theta \end{aligned} \tag{3}$$

Assuming the blade deformation as a cubic polynomial [23] and considering the boundary conditions of Eq. (3), the normalized modes are represented in Eq. (4):

$$\begin{aligned} N_1 &= \frac{3x^2}{L^2} - \frac{2x^3}{L^3} \\ N_2 &= \frac{x^3}{L^2} - \frac{x^2}{L} \end{aligned} \tag{4}$$

The dynamic modeling is derived from Lagrange's equations. For a conservative system with constant parameters, kinetic energy is given by Eq. (5), where m denotes the mass of the CWTB and $W(x)$ represents the deformation in terms of the generalized coordinates w and θ [24]:

$$T = \frac{1}{2} m \int_0^L \left(\frac{\partial W(x)}{\partial t} \right)^2 dx \tag{5}$$

The potential energy, derived from the deflection of the CWTB, is given by Eq. (6), where k is the deflection curvature, E is the modulus of elasticity, and I is the inertia moment of the cross-section [7]:

$$U = \frac{EI}{2} \int_0^L k^2 dy \tag{6}$$

For large deflections of the CWTB, the square of the deflection curvature k is defined by Eq. (7) [25]:

$$k^2 \approx \left(\frac{\partial^2 W(x)}{\partial x^2} \right)^2 \left[1 - \frac{3}{2} \left(\frac{\partial W(x)}{\partial x} \right)^2 \right]^2 \tag{7}$$

Equations (5) and (6) are incorporated into the Lagrange equation. During its development, the nonlinear Eqs. (8) and (9) are obtained, where the potential-derived forces U_w and U_θ, the excitation force P, and the damping forces D_w and D_θ are explained in detail in [10]:

$$\ddot{w} = \frac{12}{m} P + \frac{66}{mL} D_\theta + \frac{12}{m} D_w - \frac{12}{m} U_w - \frac{66}{mL} U_\theta \tag{8}$$

$$\ddot{\theta} = -\frac{66}{mL} U_w - \frac{468}{mL^2} U_\theta + \frac{66}{mL} P + \frac{468}{mL^2} D_\theta + \frac{66}{mL} D_w \tag{9}$$

2.2. Calculation of sectional properties

The cross-section of the CWTB features a hollow aerodynamic profile. The structure consists of a laminated shell, formed by n layers of composite material distributed along its perimeter (Fig. 3). Each layer of the laminate is oriented in directions parallel and perpendicular to the local $u - v$ coordinate system, defined within the global $x - y$ plane. These laminates are orthotropic, with fibers aligned according to the $1 - 2$ material coordinate system, which is oriented in the $x - z$ plane.

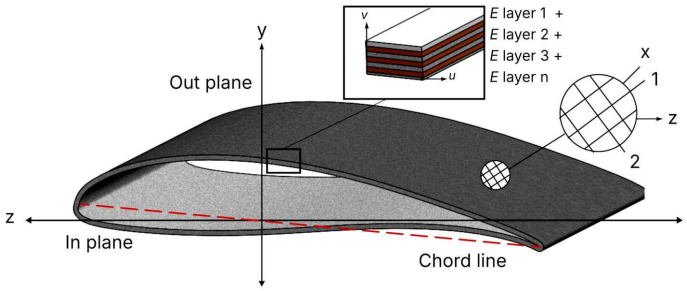

Fig. 3. CWTB cross-section and laminated plies.

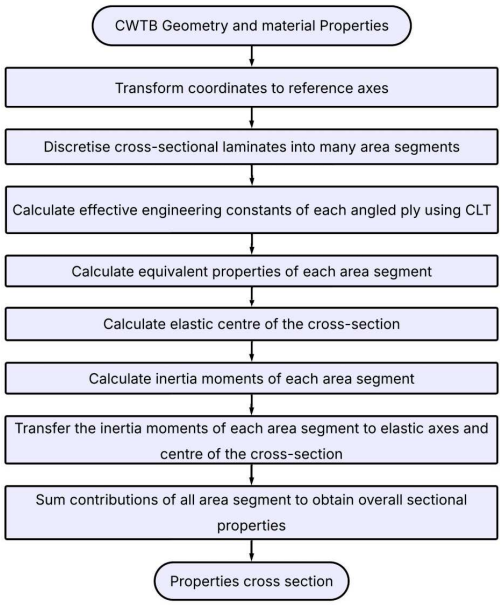

Fig. 4. Flowchart for calculating cross-section properties.

For the calculation of cross-sectional properties, this study adapts the sectional analysis methodology for laminated hollow CWTBs proposed by [15], as described in Fig. 4. This process begins by transforming all element coordinates into a global reference coordinate system. Next, the cross-section laminates are discretized into area segments, each with layers oriented in a local $u-v$ plane. For each layer, its effective elastic constants in the longitudinal x and transverse $y-z$ directions are calculated using the CLT, allowing characterization of the unidirectional contribution.

Using the weighting method [26], the equivalent properties of each segment and the location of the elastic center of the cross-section are obtained. Subsequently, the inertia moments of each segment about its local axes and centroid are calculated. These are then transferred to the system of elastic axes and the section center using coordinate transformations and the parallel axis theorem. The sum of the contributions from all segments yields the sectional properties.

2.3. Equivalent beam calculation

The CWTB features complex geometry, with a cross-section that varies from the root to the tip. Each segment along its length possesses a specific number of laminate layers, resulting in unique sectional properties at every point. This configuration allows the CWTB to be modeled as a beam with a variable cross-section, where each i-th section of length L_i has an associated inertia moment I_i. This model is represented in Fig. 5.

When the variable cross-section beam is subjected to a bending moment M, the bending slope is defined as Eq. (10):

$$\theta = \frac{M}{E}\left(\frac{L_1}{I_1}+\frac{L_2}{I_2}+\cdots+\frac{L_i}{I_i}+\cdots+\frac{L_n}{I_n}\right)=\frac{M}{E}\sum_{i=1}^{n}\frac{L_i}{I_i} \tag{10}$$

For an equivalent beam, the bending slope is given by Eq. (11):

$$\theta = \frac{ML}{EI_e} \tag{11}$$

Assuming a constant of elasticity modulus E and an equal bending slope θ, the equivalent inertia moment I_e is defined by Eq. (12):

$$I_e = \frac{\sum_{i=1}^{n} L_i}{\sum_{i=1}^{n}\frac{L_i}{I_i}} \tag{12}$$

2.4. Experimental methodology

The test bench for the vibration analysis of cantilevered CWTB is shown in Fig. 6. In this setup, the CWTB is clamped to a rigid support at the root. Once secured, the CWTB is excited to study its behavior under free and forced vibration. This experimental setup consists of the following elements: A Kistler model 8440A5 piezoelectric accelerometer (sensitivity: 1067 $\mathrm{mV/g}$), connected to a 24 bit data acquisition system (DAQ) with a sampling rate of up to 200 kSps per channel, controlled by the KiStudio Lab Package Type 2910A software (which includes the jBEAM postprocessing software); a Kistler LabAmp 5165A4 charge amplifier for dynamic measurements, with four channels. A motor is excited by a Variable Frequency Drive (VFD) operating over a range of 28 to 60 Hz.

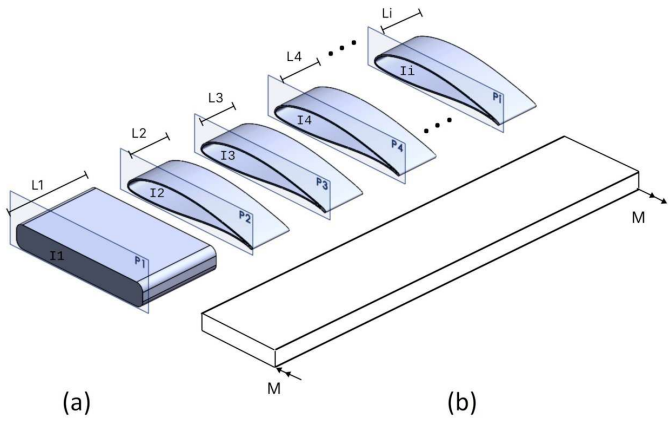

Fig. 5. Representation of the CWTB as a beam with i variable sections: (a) Sectioned CWTB, (b) Equivalent beam model of the CWTB.

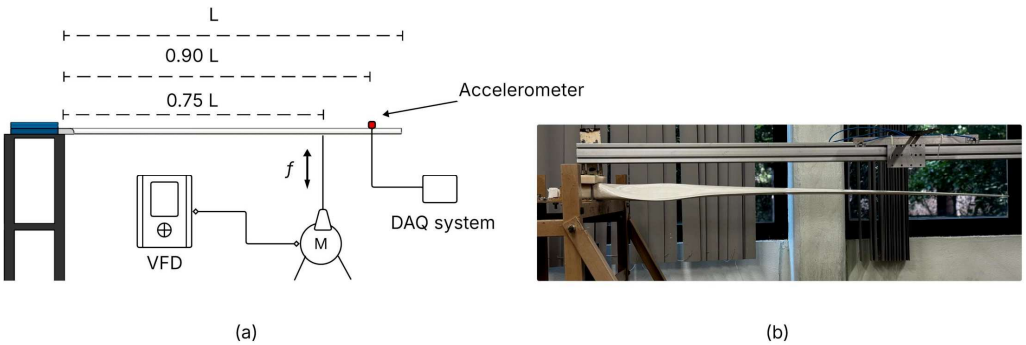

Fig. 6. Experimental setup for cantilevered CWTB vibration analysis: (a) Motor excitation system with VFD and DAQ unit, (b) Laboratory test bench.

Table 1. Distribution of epoxy resin-fiberglass laminates [15].

Layer	1	2	3	4	5	6	7	8	9	10	11	12	13	14
Thickness [mm]	0.6	0.3	0.3	0.6	0.3	0.6	0.3	0.6	0.3	0.3	0.6	0.3	0.6	0.3
Direction fiber $\frac{E_1}{E_2}$ [Deg]	45/-45	0/ 90	0/ 90	45/-45	0/ 90	45/-45	0/ 90	45/-45	0/ 90	0/ 90	45/-45	0/ 90	45/-45	0/ 90
Start [m]	0	0	0	0	0	0	0	0	0	0	0	0	0	0
End [m]	0.75	0.75	1.66	1.66	1.66	1.66	1.66	0.75	0.75	1.66	1.66	1.66	1.66	1.66

Table 2. CWTB simulation parameters.

Blade Properties	Simulation parameters			
$m = 2.7$ kg	Test	Type	Initial condition	Excitation
$L = 1.71$ m	1	Free vibration	$w_0 = 0.01$ m, $\dot{w}_0 = 0, \theta_0 = 0, \dot{\theta}_0 = 0$	$F = 0, f = 0$
$E = 16.874$ GPa	2	Free vibration	$w_0 = 0.06$ m, $\dot{w}_0 = 0, \theta_0 = 0, \dot{\theta}_0 = 0$	$F = 0, f = 0$
$I_e = 1.3953\text{x}10^{-7}\text{m}^4$	3	Forced vibration	$w_0 = 0.00$ m, $\dot{w}_0 = 0, \theta_0 = 0, \dot{\theta}_0 = 0$	$F = 10$ N, $f = 30.7$ Hz
$b = 1.97$ kg/s	4	Forced vibration	$w_0 = 0.00$ m, $\dot{w}_0 = 0, \theta_0 = 0, \dot{\theta}_0 = 0$	$F = 10$ N, $f = 48.5$ Hz

3. Results and Discussion

3.1. CWTB properties and geometry

A 1.5 kW CWTB with a length of 1.71 m and a mass of 2.7 kg is analyzed. The aerodynamic design uses the FX 63-137 airfoil profile and a chord distribution detailed in [15].

The CWTB is manufactured from layers of glass fiber composite material with an epoxy matrix, whose E-glass/epoxy density is $\rho = 1505$ kg/m^3, with elasticity modulus in the fiber direction of $E_1 = 31.3$ GPa and $E_2 = 6.05$ GPa. The laminate configuration is presented in Table 1.

The calculation of the CWTB's sectional properties yielded a longitudinal elastic modulus of $E = 16.872$ GPa. Figure 7 illustrates the distribution of the inertia moment along the length of the CWTB, revealing a pronounced, nonlinear variation that is characteristic of the variable geometry of a wind turbine blade. The behavior of the inertia moment exhibits three distinct regimes: (1) constant, (2) exponential decay, and (3) linear.

The curve descends sharply from a maximum value near the blade root at position $I(0.34\text{ m}) = 7.575\text{ x}10^{-7}$ m^4 to a minimum value in the region close to the tip, at $I(1.65\text{ m}) = 1.963\text{ x}10^{-9}$ m^4. This decrease is a direct consequence of the reduction in the chord length and the thinning of the aerodynamic profile along the blade span. The reduction in stiffness along the blade is due to a laminate with a constant elastic modulus. Therefore, the variation in the inertia moment depends solely on the cross-sectional geometry, taper, and thickness reduction, and not on the plies' stacking sequence. The equivalent inertia moment was obtained from Eq. (11), $I_e = 1.390\text{x}10^{-7}$ m^4.

3.2. Numerical simulation

The numerical solution of Eq. (8) and Eq. (9) was obtained in Matlab R2024b using the fourth-order Runge-Kutta (RK4) method. Two experimental cases were evaluated: free vibration from an initial displacement w_0 and forced vibration with frequency excitations, as specified in Table 2, where b is the viscous damping constant.

The frequency domain excitation force is defined in Eq. (12), where $\omega = 2\pi f$ and f is the frequency:

$$P = F\,sin(\omega t) \tag{12}$$

3.2.1. *Numerical free vibration*

The free vibration response of the CWTB to an initial displacement $w_0 = 0.06$ m exhibits damp linear behavior (see Fig. 8). The time domain plot (Fig. 8(a)) shows an oscillation whose acceleration $\ddot{w}$ decays exponentially from 22 m/s^2, while the frequency spectrum (Fig. 8(b)) reveals a single, well-defined peak at 7.5 Hz, corresponding to the system's natural frequency.

Figure 9 shows the phase portraits for the free vibration of the CWTB, initiated by a $w_0 = 0.01$ m displacement. The plot reveals a smooth, elliptical trajectory. The concentric, decaying nature of the cycles is characteristic of a damped harmonic oscillator, indicating progressive energy dissipation.

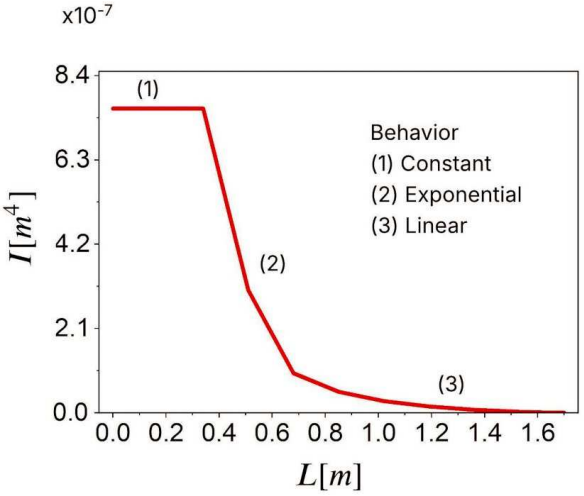

Fig. 7. Distribution of transverse inertia moment along the length of the 1.5 kW CWTB.

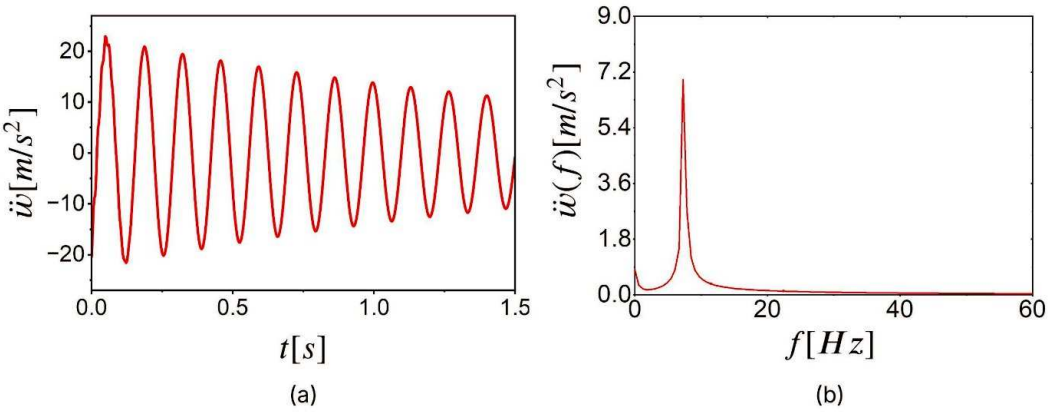

Fig. 8. Numerically simulated free vibration of the CWTB excited by an initial tip displacement of 0.01 m: (a) Time-domain acceleration, (b) Frequency spectrum.

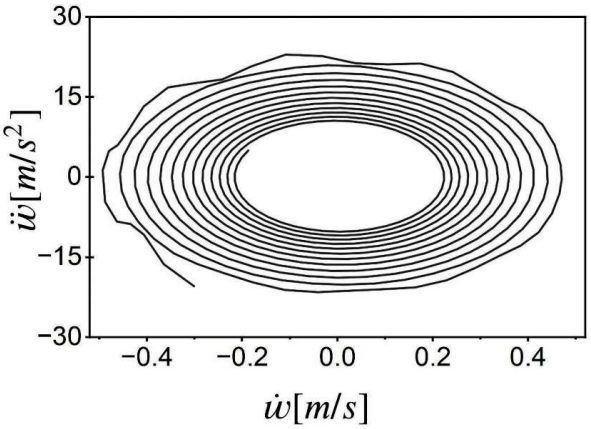

Fig. 9. Numerical phase portrait of the CWTB under free vibration from an initial displacement of 0.01 m.

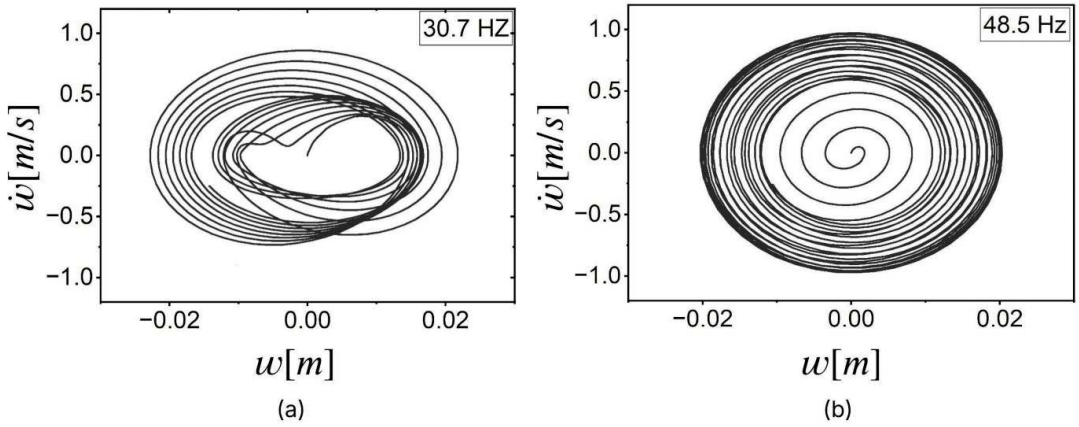

Fig. 10. Numerical phase portraits of the CWTB under simulated forced vibration: (a) For an exciting force at 30.7 Hz, (b) For an exciting force at 48.5 Hz.

3.2.2. *Numerical forced vibration*

Figure 10 shows the phase portraits of the CWTB excited at 30.7 Hz and 48.5 Hz. The curve in the phase portrait of Fig. 10(a) exhibits elongated, closed cycles with asymmetry between the positive and negative lobes, characterized by a narrowing at the points of maximum deflection w and variable curvature. These features indicate the presence of nonlinear stiffness in the system. The maximum values are ±0.025 m for deflection w and ±0.75 m/s for velocity $\dot{w}$, generated by the excitation at 30.7 Hz, which activates a superharmonic corresponding to four times the system's natural frequency (4 × 7.5 Hz = 30 Hz). At this maximum deflection, the curve narrows, indicating strain stiffening [27]. This phenomenon reflects that the stiffness of the CWTB increases nonlinearly under large deflections.

The Phase portrait of Fig. 10(b) captures the nonlinear resonance of the CWTB excited at 48.5 Hz, corresponding to its third natural frequency. It exhibits accelerated growth in displacement from the center, forming a radial expansion. The asymmetry of the closed orbit denotes the presence of geometric nonlinearities, accompanied by a progressive narrowing of the trajectory as the deflection increases. The outer boundary represents the resonant steady state, where the high density of cycles confirms the stability of this peripheral attractor. The system remains in this state for the majority of the time after overcoming the initial transient.

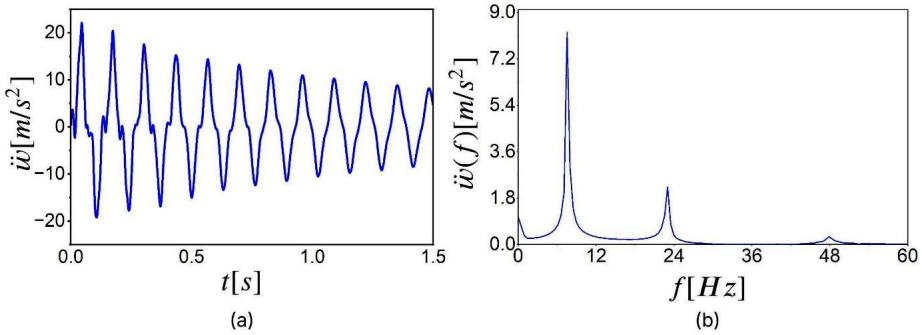

Fig. 11. Experimental free vibration response of the CWTB excited by an initial displacement of 0.01 m: (a) Acceleration in the time domain, (b) Frequency spectrum.

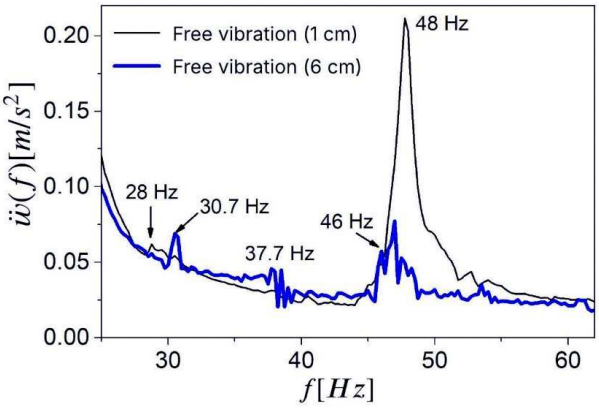

Fig. 12. Experimental frequency spectrum comparing linear (initial displacement of 0.01 m) and nonlinear (initial displacement of 0.06 m) free vibration regimes.

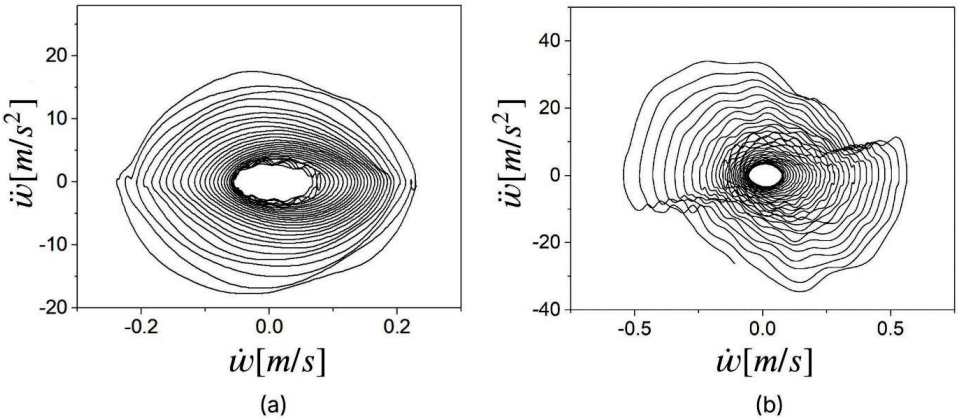

Fig. 13. Experimental phase portraits of the free vibration response under different energy regimes: (a) Low initial displacement (0.01 m), (b) High initial displacement (0.06 m).

3.3. Experimental vibration response

3.3.1. *Experimental free vibration*

Figure 11 shows the free vibration response of the CWTB. Figure 11(a) displays a decaying oscillation, characteristic of a damped system. Following excitation, the CWTB vibrates at its natural frequencies, but the material's energy dissipation gradually reduces the vibration acceleration $\ddot{w}$. The complex, non-sinusoidal waveform indicates the presence of multiple superimposed vibrational frequencies.

These frequencies are shown in Fig. 11(b), which presents the vibration spectrum. The peaks correspond to the resonant modes of the CWTB: the fundamental mode at 7.5 Hz with the highest amplitude $\ddot{w}(f)$, followed by modes at 23.5 Hz and 48.5 Hz.

To characterize its response at large deflections, the CWTB was subjected to free vibration until it reached rest. The study contrasted linear and nonlinear behavior using two initial displacements, w_0: a low deflection (0.01 m, 0.65% of the length) and a high deflection (0.06 m, 3.9%).

Figure 12 characterizes this behavior at high frequencies (above 25 Hz), revealing a clear distinction between the two regimes. Under low deflection conditions, the 48.5 Hz natural frequency dominates, with the highest amplitude $\ddot{w}(f)$, and is accompanied by a 28 Hz component. In contrast, under large deflections, the spectrum is enriched by new spectral components at 30.7 Hz, 37.7 Hz, and 47 Hz with reduced amplitudes $\ddot{w}(f)$, indicating the activation of nonlinear modes. The linear mode at 48.5 Hz is abruptly suppressed under large deflections, exhibiting reduced amplitude and a slight shift to 47 Hz, confirming an alteration in the system's effective stiffness due to nonlinear effects. This behavior is accompanied by spectral broadening, where vibrational energy disperses into frequency bands adjacent to the natural modes.

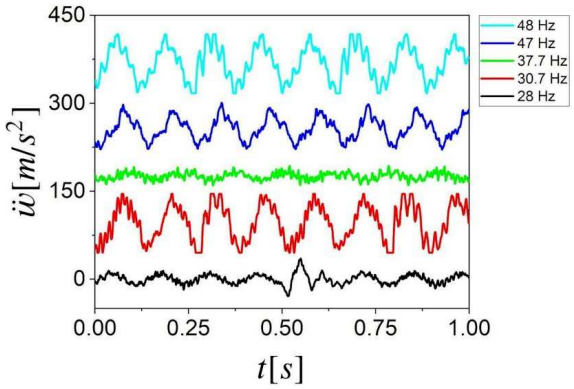

Fig. 14. Experimental forced vibration responses of the CWTB under harmonic excitation at discrete frequencies (28 Hz, 30.7 Hz, 37.7 Hz, 47 Hz, and 48.5 Hz).

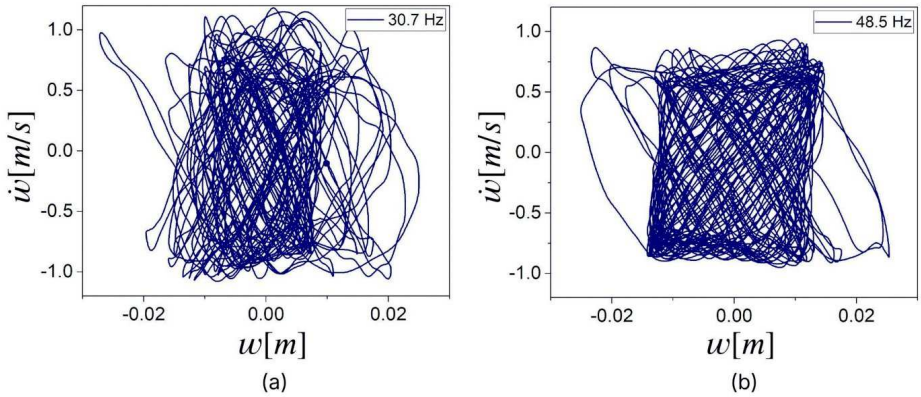

Fig. 15. Experimental phase portraits under forced harmonic excitation. (a) Response to 30.7 Hz excitation. (b) Response to 48.5 Hz excitation.

Figure 13 characterizes the nonlinear behavior of the CWTB through phase portraits, obtained by numerically integrating the acceleration $\ddot{w}$, to calculate velocity $\dot{w}$. The phase portrait in Fig. 13(a) corresponds to a free vibration with low initial displacement (0.01 m). In this low-energy regime, the system dynamics are predictable and described by a smooth, closed oval trajectory, typical of a linear system or one with very mild nonlinearities. In contrast, the phase portrait in Fig. 13(b) results from a high initial displacement condition (0.06 m), which drives the system into a high-energy regime. Here, the response becomes entirely distorted, giving rise to a complex, aperiodic structure suggestive of chaotic behavior. In this nonlinear state, the central region around the equilibrium point (acceleration $\ddot{w} \approx 0$ and velocity $\dot{w} \approx 0$) retains a defined oval shape. This condition indicates that linear behavior persists during small oscillations, albeit masked by the strong nonlinearity governing the high amplitude response.

3.3.2. *Experimental forced vibration*

Figure 14 shows the response of the CWTB subjected to forced vibration. The system's response to different excitation frequencies is observed: 28 Hz, 30.7 Hz, 37.7 Hz, 47 Hz, and 48.5 Hz.

The vibrational response of the CWTB shows a high acceleration $\ddot{w}$ amplitude when excited near its natural frequency (47–48.5 Hz), indicating typical resonant behavior. However, an anomaly is observed when forced at 30.7 Hz; the vibration acceleration reaches high values, even exceeding the linear resonance range. The signal at 30.7 Hz exhibits apparent nonlinear distortion, with a non-sinusoidal waveform, featuring flattened peaks and inter-cycle asymmetry. This signal is consistent with the activation of this higher frequency by energy from the 23.5 Hz resonance. At 28 Hz, the system responds with low acceleration $\ddot{w}$ and a sinusoidal waveform, typical of a linear regime. At 37.7 Hz, the acceleration $\ddot{w}$ increases, and nonlinear distortion begins, marking an energetic transition between the 23.5 Hz and 48.5 Hz resonant frequencies.

Figure 15 shows the velocity $\dot{w}$-deflection w phase portraits of the CWTB forced to vibrate at 30.7 Hz and 48.5 Hz, both exhibiting high amplitude dynamic behavior. The phase orbit at 30.7 Hz in Fig. 15(a) reveals a complex nonlinear response, with multiple crossings and overlapping loops indicating non-periodicity. Its asymmetry between half cycles suggests asymmetric stiffness (tension or compression-stiffening), while localized flattening indicates nonlinear restoring forces. The variable width of the trajectory indicates damping associated with material hysteresis. This behavior is activated because 30.7 Hz coincides with two nonlinear resonant mechanisms: it acts as a sum frequency (23.5 Hz + 7.5 Hz ≈ 30.7 Hz), coupling modes 1 and 2 through geometric nonlinearities, and simultaneously triggers a 3/2 subharmonic response (2/3·48.5 Hz ≈ 32 Hz), thereby exciting the third mode (48.5 Hz) [28-29]. This dual synchronization triggers a multisystem modal interaction, where the superposition of modes (7.5 Hz, 23.5 Hz, and 48.5 Hz) generates the observed quasi-chaotic signature.

In Fig. 15(b), the trajectories exhibit distortions and flattening, deviating from perfect ellipses. The asymmetry between the positive and negative halves of the cycle in some orbits suggests the presence of nonlinear stiffness induced by large deformations. The superposition of multiple loops describes a non-periodic response. Furthermore, the variable width of the orbit indicates nonlinear, velocity-dependent damping. These nonlinearities, activated by large deflections w (up to ±0.023 m), result in distinctly nonlinear behavior even when the excitation is at the fundamental frequency.

4. Conclusions

This study analyzed the nonlinear dynamic behavior of a CWTB using an experimentally validated equivalent beam model that efficiently and accurately captures geometric nonlinearities arising from large deflections.

Under large deflections, the CWTB exhibited nonlinear stiffening, as evidenced by spectral broadening, the activation of superharmonic resonances, and shifts in natural frequencies. Free vibration tests confirmed nonlinear modal coupling under large initial displacements (0.06 m), manifested by the emergence of spectral components at 30.7 Hz and 37.7 Hz and by a reduction in the 48.5 Hz mode. In addition, phase portraits under forced vibration revealed complex dynamics, featuring asymmetric orbits, multiple loops, and non-periodic responses, particularly at 30.7 Hz, a frequency linked to internal resonances and subharmonic interactions.

The integration of sectional properties via CLT enables a reliable CWTB model that accounts for the laminate layer distribution and provides an efficient approximation of the elastic modulus. This approach significantly reduces computational cost by consolidating the properties into a one-dimensional equivalent beam model. Hence, the proposed equivalent beam model, derived from variable sectional properties and CLT, effectively predicted both the linear (error < 1%) and nonlinear (error < 8.6%) responses of the CWTB, demonstrating good numerical-experimental agreement. While these findings validate the method's reliability for assessing the CWTB's nonlinear behavior, future work should investigate the interactions among the laminate layers and their influence on structural damping.

Author Contributions

A. Lopez-Lopez developed the mathematical modeling and examined the theory validation; R.M. Sánchez-Albores planned the scheme, initiated the project, and suggested the experiments; P.Y. Sevilla-Camacho conducted the experiments and analyzed the empirical results; H.H. Torres-Ventura developed the simulation code; J. Rodríguez-Reséndiz validated the experiments; J.B. Robles-Ocampo supervised and managed the project. The manuscript was written through the contribution of all authors. All authors discussed the results, reviewed, and approved the final version of the manuscript.

Acknowledgments

The authors would like to acknowledge the Secretaría de Ciencia, Humanidades, Tecnología e Innovación (SECIHTI), and the Sistema Nacional de Investigadores e Investigadoras (SNII) for their support.

Conflict of Interest

The authors declared no potential conflicts of interest concerning the research, authorship, and publication of this article.

Funding

This research received no external funding.

Data Availability Statements

The datasets generated and/or analyzed during the current study are available from the corresponding author on reasonable request.

Nomenclature

b	Viscous damping constant [kg/s]	P	Excitation force [N]
D_w	Damping force derivative with respect to deflection [N]	F	Force amplitude [N]
D_θ	Damping force derivative with respect to bending slope [Nm].	q_i	Generalized coordinates (i = 1, 2, 3, …, *n*)
E	Modulus of elasticity [Pa]	t	Time [s]
E_1	Modulus of elasticity direction 1 [Pa]	T	Kinetic energy [J]
E_2	Modulus of elasticity direction 2 [Pa]	U	Potential energy [J]
I	Moment of inertia [m^4]	U_w	Potential-derived force with respect to deflection
I_e	Equivalent Moment of inertia [m^4]	U_θ	Potential-derived force with respect to bending slope [Nm]
I_i	I-th moment of inertia of the cross-section [m^4] (i = 1, 2, 3, …, *n*)	W	Vector deformation of the flexible cantilever blade
k	Deflection curvature	w, w_1, w_2	Flapwise deflection and deflection nodes [m]
L	Length [m]	$\dot{w}$	Flapwise velocity [m/s]
L_i	I-th length [m] (i = 1, 2, 3, …, *n*)	$\ddot{w}$	Flapwise acceleration [m/s^2]
m	Mass [kg]	x, y, z	General reference coordinates
M	Bending moment [N.m]	$\theta, \theta_1, \theta_2$	Bending slope and bending slope nodes [rad]
N_i	Normalized modes	$\ddot{\theta}$	Acceleration angular [rad/s^2]

References

[1] Wang, Y., Cai, C., Liao, C., Hu, Z., Zhang, L., Sun, X., Zhong, X., Li, Q., Aeroelastic Stability Analysis of Large-Scale Wind Turbine Blades under Different Operating Conditions Based on System Identification and Floquet Theory, *Energy*, 326, 2025, 136279.
[2] Mo, W., Li, D., Wang, X., Zhong, C., Aeroelastic Coupling Analysis of the Flexible Blade of a Wind Turbine, *Energy*, 89, 2015, 1001–1009.
[3] Zuo, H., Bi, K., Hao, H., A State-of-the-Art Review on the Vibration Mitigation of Wind Turbines, *Renewable and Sustainable Energy Reviews*, 121, 2020, 109710.
[4] Sahoo, S., Kushwah, K., Sunaniya, A.K., Health Monitoring of Wind Turbine Blades through Vibration Signal Using Advanced Signal Processing Techniques, *Proceedings of the 2020 Advanced Communication Technologies and Signal Processing (ACTS)*, 2020, 1–6.
[5] Della Posta, G., Leonardi, S., Bernardini, M., A Two-Way Coupling Method for the Study of Aeroelastic Effects in Large Wind Turbines, *Renewable Energy*, 190, 2022, 971–992.
[6] Xu, J., Zhang, L., Li, X., Li, S., Yang, K., A Study of Dynamic Response of a Wind Turbine Blade Based on the Multi-Body Dynamics Method, *Renewable Energy*, 155, 2020, 358–368.
[7] Gonzalez-Cruz, C.A., Jauregui-Correa, J.C., Herrera-Ruíz, G., Nonlinear Response of Cantilever Beams Due to Large Geometric Deformations: Experimental Validation, *Strojniski Vestnik/Journal of Mechanical Engineering*, 62, 2016, 187–196.
[8] Karimi, B., Moradi, H., Nonlinear Kinematics Analysis and Internal Resonance of Wind Turbine Blade with Coupled Flapwise and Edgewise Vibration Modes, *Journal of Sound and Vibration*, 435, 2018, 390–408.

[9] Lang, Q., Zheng, Y., Cui, T., Shi, C., Zhang, H., Nonlinear Flap-Wise Vibration Characteristics of Wind Turbine Blades Based on Multi-Scale Analysis Method, *Energy Engineering*, 121, 2024, 483–498.
[10] Lopez-Lopez, A., Robles-Ocampo, J.B., Sevilla-Camacho, P.Y., Lastres-Danguillecourt, O., Muniz, J., Perez-Sariñana, B.Y., de la Cruz, S., Dynamic Instability of a Wind Turbine Blade Due to Large Deflections: An Experimental Validation, *Strojniski Vestnik/Journal of Mechanical Engineering*, 66, 2020, 523–533.
[11] Tüfekci, M., Genel, Ö.E., Tatar, A., Tüfekci, E., Dynamic Analysis of Composite Wind Turbine Blades as Beams: An Analytical and Numerical Study, *Vibration*, 4, 2021, 1–15.
[12] Xue, Z., Zhang, H., Ji, Y., Dynamic Response of a Flexible Multi-Body in Large Wind Turbines: A Review, *Sustainability*, 15, 2023, 6590.
[13] Navadeh, N., Goroshko, I., Zhuk, Y., Etminan Moghadam, F., Soleiman Fallah, A., Finite Element Analysis of Wind Turbine Blade Vibrations, *Vibration*, 4, 2021, 310–322.
[14] Jokar, H., Mahzoon, M., Vatankhah, R., Dynamic Modeling and Free Vibration Analysis of Horizontal Axis Wind Turbine Blades in the Flap-Wise Direction, *Renewable Energy*, 146, 2020, 1818–1832.
[15] Lopez-Lopez, A., Robles-Ocampo, J.B., Lastres-Danguillecourt, O., Ibañez, G., Hernandez-Estrada, E., Sevilla-Camacho, P.Y., Novel Method for Determination the Dynamic Elastic Modulus of Composite Wind Turbine Blades, *Engineering Structures*, 312, 2024, 118254.
[16] Ou, Y., Chatzi, E.N., Dertimanis, V.K., Spiridonakos, M.D., Vibration-Based Experimental Damage Detection of a Small-Scale Wind Turbine Blade, *Structural Health Monitoring*, 16, 2017, 79–96.
[17] Aranizadeh, A., Shad, H., Vahidi, B., Khorsandi, A., A Novel Small-Scale Wind-Turbine Blade Failure Detection According to Monitored-Data, *Results in Engineering*, 25, 2025, 103809.
[18] Su, R., Gao, Z., Chen, Y., Bai, Y., Wang, J., Experimental on the Fatigue Failure Areas of Wind Turbine Blades' Rotating Fundamental Frequency, *AIP Advances*, 13, 2023, 065123.
[19] Jiménez, C.A., Hernández Gálvez, G., Dorrego Portela, J.R., Verde Añorve, A., Ibáñez Duharte, G., Pantoja Enríquez, J., Lastres Danguillecourt, O., Perea-Moreno, A.-J., Muñoz-Rodriguez, D., Hernandez-Escobedo, Q., Sustainable Analysis of Wind Turbine Blade Fatigue: Simplified Method for Dynamic Load Measurement and Life Estimation, *Sustainability*, 17, 2025, 7615.
[20] Sevilla-Camacho, P.Y., Robles-Ocampo, J.B., Rodríguez-Resendíz, J., De la Cruz-Arreola, S., Zuñiga-Reyes, M.A., Hernández-Estrada, E.N., Crack Location in Wind Turbine Blades Using Vibration Signal and Support Vector Machine, *Vibration*, 8, 2025, 20.
[21] Ou, Y., Tatsis, K.E., Dertimanis, V.K., Spiridonakos, M.D., Chatzi, E.N., Vibration-Based Monitoring of a Small-Scale Wind Turbine Blade under Varying Climate Conditions. Part I: An Experimental Benchmark, *Structural Control and Health Monitoring*, 28, 2021, e2660.
[22] Jin, X., Liu, H., Ju, W., Wind Turbine Seismic Load Analysis Based on Numerical Calculation, *Strojniski Vestnik/Journal of Mechanical Engineering*, 60, 2014, 638–648.
[23] Gerstmayr, J., Irschik, H., On the correct representation of bending and axial deformation in the absolute nodal coordinate formulation with an elastic line approach, *Journal of Sound and Vibration*, 318(3), 2008, 461-487.
[24] Tang, A.-Y., Li, X.-F., Wu, J.-X., Lee, K.Y., Flapwise Bending Vibration of Rotating Tapered Rayleigh Cantilever Beams, *Journal of Constructional Steel Research*, 112, 2015, 1–9.
[25] Maktouf, R., Yangui, M., Fakhfekh, T., Nasri, R., Haddar, M., Non-Linear Dynamic Analysis of a Wind Turbine Blade, *Journal of the Chinese Institute of Engineers, Transactions of the Chinese Institute of Engineers, Series A*, 42, 2019, 727–737.
[26] Wang, L., Liu, X., Guo, L., Renevier, N., Stables, M., A Mathematical Model for Calculating Cross-Sectional Properties of Modern Wind Turbine Composite Blades, *Renewable Energy*, 64, 2014, 52–60.
[27] Wang, Z., Lu, Z., Yi, W., Hao, J., Chen, Y., A Study of Nonlinear Aeroelastic Response of a Long Flexible Blade for the Horizontal Axis Wind Turbine, *Ocean Engineering*, 279, 2023, 113660.
[28] Yuan, G., Wang, Y., Internal, Primary and Combination Resonances of a Wind Turbine Blade with Coupled Flapwise and Edgewise Motions, *Journal of Sound and Vibration*, 514, 2021, 116439.
[29] Li, L., Li, Y.H., Lv, H.W., Liu, Q.K., Flapwise Dynamic Response of a Wind Turbine Blade in Super-Harmonic Resonance, *Journal of Sound and Vibration*, 331, 2012, 4025–4044.

ORCID iD

Andres Lopez-Lopez https://orcid.org/0000-0001-5707-9395
Rocio M. Sánchez-Albores https://orcid.org/0000-0002-5197-0125
Perla Y. Sevilla-Camacho https://orcid.org/0000-0002-9702-1929
Héctor H. Torres-Ventura https://orcid.org/0000-0002-7357-6524
Juvenal Rodríguez-Reséndiz https://orcid.org/0000-0001-8598-5600
José B. Robles-Ocampo https://orcid.org/0000-0002-0094-8710

© 2026 Shahid Chamran University of Ahvaz, Ahvaz, Iran. This article is an open access article distributed under the terms and conditions of the Creative Commons Attribution-NonCommercial 4.0 International (CC BY-NC 4.0 license) (http://creativecommons.org/licenses/by-nc/4.0/).

How to cite this article: Lopez-Lopez A. et al., Nonlinear Dynamic Analysis of Composite Wind Turbine Blades using Lamination and Equivalent Beam Theory, *J. Appl. Comput. Mech.*, 12(4), 2026, 1535-1545.
https://doi.org/10.22055/jacm.2026.48947.5616

Publisher's Note Shahid Chamran University of Ahvaz remains neutral with regard to jurisdictional claims in published maps and institutional affiliations.